Eco-Friendly Synthesis of Ag-Doped $MgFe_2O_4$ Nanoferrites with Enhanced Photocatalytic Properties

[1]Vijay Luxmi, [2]Rimple, [3]Ashish

[1]Assistant Professor, [2]Research Scholar, [3]Assistant Professor
[1,2]Department of Physics,
[1,2]IEC University, Baddi, India
[3]Department of Mathematics,
[3]Smt AAA Govt. P.G. College, Kalka, India

Abstract : In the present work, pure and Ag-doped magnesium ferrite ($MgFe_2O_4$) nanoparticles were synthesized and studied for their structural, optical, surface, morphological, and photocatalytic properties. X-ray diffraction analysis confirmed the formation of cubic spinel ferrite structure with a prominent (311) reflection peak. The crystallite size decreased from 31.8 nm to 17.6 nm with increasing Ag concentration, indicating that Ag doping suppresses crystal growth. The lattice parameter remained nearly constant in the range of 8.38–8.39 Å, while slight variations in microstrain suggested lattice distortion due to dopant incorporation. SEM observations confirmed spherical nano-sized particles with increased agglomeration at higher Ag concentration.

BET surface area analysis revealed improved textural properties after doping. The specific surface area increased from 30.2 m^2/g for the pure sample to 40.3 m^2/g for the doped sample, accompanied by enhanced pore volume, confirming the mesoporous nature of the nanoparticles. UV–Visible spectroscopy showed strong absorption in the visible region with band gap energies varying from ~2.1 to 2.06 eV. The reduction in band gap energy after doping indicates enhanced visible-light absorption capability.

Photocatalytic studies using Congo Red dye under visible-light irradiation demonstrated significant enhancement in degradation efficiency after Ag doping. Among all samples, 6% doping of Ag showed the highest photocatalytic degradation efficiency of 99.7% within 150 minutes. The enhanced performance is mainly attributed to reduced crystallite size, higher surface area, improved porosity, and better visible-light response. These results suggest that Ag-doped $MgFe_2O_4$ nanoparticles are promising materials for environmental remediation and wastewater treatment applications.

IndexTerms **- Ag-doped $MgFe_2O_4$, Green synthesis, Spinel ferrites, Photocatalysis, Congo Red degradation, Environmental remediation.**

1. INTRODUCTION

The textile industry widely employs synthetic dyes during the dyeing process, many of which are carcinogenic in nature. Globally, nearly 20% of the total dye produced is lost during processing, leading to the continuous discharge of large volumes of dye-containing effluents into the environment. These effluents pose serious ecological threats by hindering oxygen dissolution and limiting sunlight penetration in water bodies [1-3]. As a result, aquatic ecosystems are severely affected. Moreover, prolonged exposure to such dyes has been associated with serious health disorders, including lung cancer, skin cancer, blood cancer, bladder cancer, and genetic mutations. Consequently, the effective removal and degradation of these hazardous dyes has become an urgent environmental priority [4-6].

Among various treatment techniques, photocatalysis has emerged as a highly efficient and sustainable method for dye degradation. Photocatalysts are cost-effective and can be reused, making them particularly advantageous for wastewater treatment applications [6-10]. In recent years, nanocrystalline spinel ferrites have attracted considerable interest in nanotechnology due to their unique physicochemical properties. Their high surface-to-volume ratio imparts superior characteristics compared to bulk materials, enabling their use in diverse applications such as magnetic refrigeration, ferrofluids, magnetically guided drug delivery, high-density data storage, microwave devices, computer memory systems, magnetic recording, and photocatalysis [11-15].

Magnesium ferrite ($MgFe_2O_4$), a typical spinel ferrite, is recognized as a promising photocatalyst owing to its excellent chemical stability, relatively large surface area, and narrow band gap. Its highly negative conduction band potential facilitates the generation of positively charged holes (h^+) with strong oxidizing ability. However, its limited sunlight absorption and low quantum efficiency restrict its overall photocatalytic performance. To overcome these drawbacks, modification through doping with suitable materials is often employed to enhance its efficiency [16-20].

Soft magnetic ferrites are of great academic and industrial importance. In the spinel lattice, Mg^{2+} and Fe^{3+} ions occupy tetrahedral (A) and octahedral (B) sites, and the magnetic and electromagnetic properties are governed by the interactions within and between these sublattices. Introducing dopants into the host lattice creates controlled defects, which can significantly influence photocatalytic behavior. Careful selection of dopant materials is crucial due to concerns regarding metal toxicity. Silver (Ag), considered relatively eco-friendly, possesses antimicrobial and antioxidant properties, making it a suitable dopant candidate. The incorporation of Ag can introduce surface defects and oxygen vacancies, promoting the generation of reactive radicals and thereby accelerating dye degradation. Additionally, noble metal doping enhances visible light absorption and modifies the band gap, further improving photocatalytic activity.

Several synthesis techniques have been reported for preparing $MgFe_2O_4$ nanoparticles, including co-precipitation, hydrothermal, sol–gel, micellar, and solution combustion synthesis (SCS) methods. These approaches influence particle size, morphology, distribution, and surface characteristics.

In recent years, the development of environmentally benign synthesis methods for nanomaterials has gained significant attention due to increasing concerns over toxic chemicals, high energy consumption, and hazardous by-products associated with conventional preparation techniques. Green synthesis has emerged as a sustainable alternative, utilizing biological resources such as plant extracts, microorganisms, and natural polymers as reducing, stabilizing, and capping agents. This approach minimizes environmental impact, reduces the use of harmful reagents, and offers a cost-effective and energy-efficient route for nanoparticle production [21-22].

Therefore, green-synthesized Ag-doped Fe_2O_4 nanoparticles represent a promising class of multifunctional nanomaterials combining enhanced photocatalytic efficiency with sustainable production methods. Their application in dye degradation and environmental remediation provides an effective and environmentally responsible solution to wastewater pollution.

2. Experimental Section

2.1 Chemicals Used

Magnesium nitrate hexahydrate [$Mg(NO_3)_2 \cdot 6H_2O$], ferric nitrate nonahydrate [$Fe(NO_3)_3 \cdot 9H_2O$], and silver nitrate ($AgNO_3$) were employed as precursor materials for the synthesis of silver-doped magnesium ferrite nanoparticles. Citric acid ($C_6H_8O_7$) was used as a chelating agent to facilitate complex formation and improve compositional uniformity, while ammonium hydroxide (NH_4OH) was utilized for pH adjustment during gel formation. Double-distilled water served as the solvent throughout the synthesis process. In addition to these chemicals, fresh egg white was used as a natural fuel, stabilizing, and gel-forming agent, and freshly prepared neem leaf extract was incorporated as a green reducing and capping agent to promote controlled particle growth and dopant distribution. All chemicals were of analytical grade and used without further purification.

2.2 Green synthesis of Ag–Doped $MgFe_2O_4$ Nanoparticles

Silver-doped magnesium ferrite nanoparticles ($Mg_{1-x}Ag_xFe_2O_4$) were synthesized using a modified green sol–gel auto-combustion method, employing naturally derived biomaterials to ensure an environmentally sustainable process. Magnesium nitrate hexahydrate [$Mg(NO_3)_2 \cdot 6H_2O$], ferric nitrate nonahydrate [$Fe(NO_3)_3 \cdot 9H_2O$], and silver nitrate [$AgNO_3$] were used as precursor salts without further purification.

Stoichiometric amounts of the metal nitrates were calculated based on the required composition (Mg + Ag : Fe = 1 : 2). Each salt was dissolved separately in double-distilled water to form clear aqueous solutions, which were then combined under continuous magnetic stirring to achieve uniform mixing.

In a separate preparation, fresh egg white was diluted with double-distilled water in a 3:1 volume ratio and stirred vigorously to produce a homogeneous protein solution. To introduce an additional green component and enhance nanoparticle stabilization, a small volume of freshly prepared plant extract (neem extract) was added to the protein matrix. This extract acts as a natural reducing and capping agent, facilitating controlled incorporation of silver ions.

The mixed metal nitrate solution was slowly added to the biomaterial solution under constant stirring and maintained for approximately 4 hours to ensure homogeneous distribution of all components at the molecular level. Citric acid was subsequently introduced in an equimolar ratio with respect to the total metal ions to promote complex formation and improve compositional uniformity. The pH of the resulting mixture was adjusted to approximately 7 using ammonium hydroxide (NH_4OH), enabling controlled gel formation.

The solution was then heated at 80–90 °C with continuous stirring until a viscous sol was formed. Further heating led to the formation of a dense gel as solvent evaporation progressed. Upon continued thermal treatment, the gel underwent a spontaneous combustion reaction driven by the organic constituents, producing a voluminous and porous precursor powder. The as-formed powder was gently ground and calcined at temperatures ranging from 550 to 750 °C for 2–3 hours in a muffle furnace to obtain crystalline Ag–doped $MgFe_2O_4$ nanoparticles.

In this synthesis approach, egg white serves as a natural fuel, stabilizer, and gel-forming agent, while the plant extract contributes to reduction and surface stabilization. The combined use of these green materials supports uniform dopant distribution, controlled particle growth, and reduced agglomeration, making the method efficient and environmentally friendly.

2.3 Characterization

The structural properties and phase formation of the synthesized photocatalysts were analyzed using powder X-ray diffraction (XRD) employing a Rigaku MiniFlex diffractometer. The surface morphology and particle distribution of the prepared samples were investigated through scanning electron microscopy (SEM, JEOL JSM-6390LV). Optical absorption behavior of the powdered materials was examined using a UV–visible spectrophotometer (Cary 300, Agilent Technologies). The photocatalytic degradation of dye solutions was monitored by recording absorption spectra with an M550 Camspec UV–Vis spectrometer at regular intervals. Furthermore, the specific surface area along with pore size distribution of the synthesized nanoparticles was evaluated using Brunauer–Emmett–Teller (BET) analysis carried out on a Quantachrome Nova 2200 surface area analyzer.

2.4 Photocatalytic Studies

The photocatalytic activity of the synthesized samples was evaluated using a cylindrical photocatalytic reactor (Model PMPC-250, PMI, India) consisting of three concentric compartments. For the degradation experiments, a catalyst suspension was prepared by adding 1 g/L of the synthesized photocatalyst to 50 mL of Congo red (CR) dye solution with an initial concentration of 10 mg/L. The mixture was subjected to ultrasonication for approximately 1 hour to achieve uniform dispersion of catalyst particles in the dye solution.

Following dispersion, the suspension was placed in the outer chamber of the reactor and stirred magnetically in dark conditions for 30 minutes to attain adsorption–desorption equilibrium between the dye molecules and catalyst surface. A 500 W halogen lamp positioned in the innermost chamber served as the visible light irradiation source. To maintain a stable reaction temperature and avoid overheating during illumination, continuous water circulation was provided through the middle chamber of the reactor.

During irradiation, 2 mL aliquots were collected at 30-minute intervals for analysis. The sampling process was continued until significant discoloration of the dye solution was observed. The remaining dye concentration at each interval was determined using a UV–visible spectrophotometer, and the photocatalytic degradation efficiency was subsequently evaluated.

3. RESULTS AND DISCUSSION

3.1 XRD ANALYSIS OF PURE AND AG-DOPED MGFE$_2$O$_4$ NANOPARTICLES

The XRD patterns of pure $MgFe_2O_4$ and Ag-doped $MgFe_2O_4$ nanoparticles as shown in Figure 1 display well-defined diffraction peaks corresponding to the cubic spinel ferrite structure. The prominent reflections observed at approximately 2θ values of 30°, 35°, 43°, 53°, 57°, and 62° are indexed to the (220), (311), (400), (422), (511), and (440) planes, respectively, confirming the formation of single-phase cubic spinel structure of $MgFe_2O_4$. Among these, the (311) peak exhibits the highest intensity, indicating good crystallinity of the synthesized nanoparticles.

With the incorporation of silver, additional low-intensity diffraction peaks appear around 38° and 44°, which are attributed to the (111) and (200) planes of metallic silver. These peaks confirm the successful incorporation of Ag into the $MgFe_2O_4$ matrix without altering the fundamental spinel structure. Moreover, slight peak broadening is observed in Ag-doped samples, suggesting a reduction in crystallite size and the formation of nanoscale particles.

A minor shift in peak positions is also detected with increasing Ag concentration, which may be associated with lattice strain arising from ionic size mismatch between Mg^{2+} and Ag^{+} ions. Additionally, a slight decrease in peak intensity for doped samples indicates the introduction of structural defects and enhanced surface activity.

Importantly, no extra impurity peaks were observed in any of the synthesized samples, confirming the phase purity of the materials. This indicates that the green synthesis approach using natural biomaterials provides controlled nucleation and uniform growth, leading to highly pure Ag-doped $MgFe_2O_4$ nanoparticles. The absence of secondary phases further supports the effectiveness of the eco-friendly synthesis method in producing structurally stable and homogeneous photocatalytic materials.

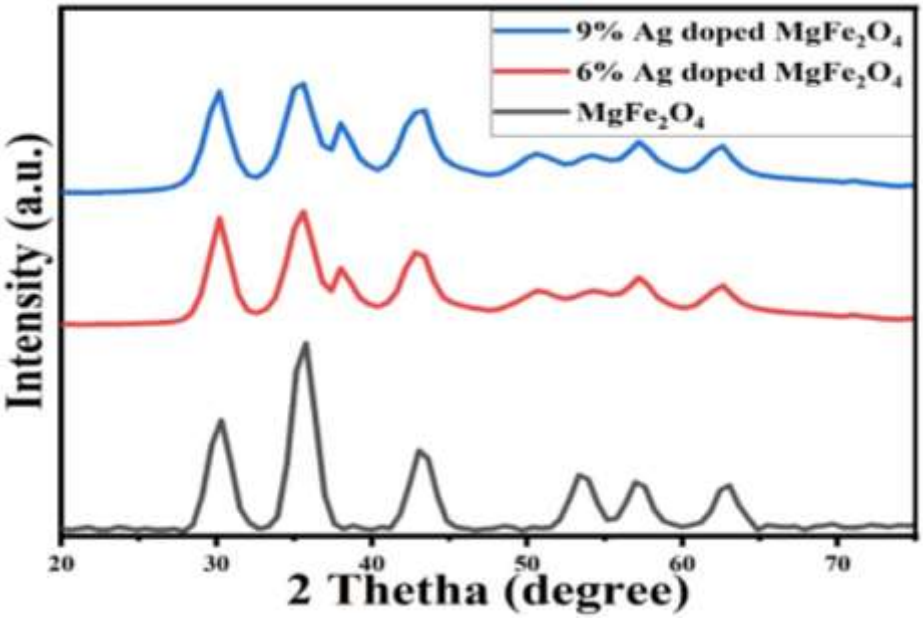

Figure 1: XRD Patterns of the pure and Ag-doped $MgFe_2O_4$ samples

Table:1 Calculated parameters using XRD patterns

Samples	2θ (°) for (311)	FWHM (β, rad)	Crystallite Size (D, nm)	Lattice Parameter (a, Å)	Microstrain (ε ×10^{-3})
A1	35.6	0.0045	31.8	8.386	2.35
A2	35.46	0.0074	20.2	8.38	2.08
A3	35.41	0.0086	17.6	8.39	2.41

3.2 SEM Analysis

The surface morphology of pure and Ag-doped $MgFe_2O_4$ nanoparticles was investigated using scanning electron microscopy, and the corresponding micrographs are presented in Figure 2 (A1–A3). The SEM image of pure $MgFe_2O_4$ (A1) shows nearly spherical nanoparticles with relatively uniform size distribution. The particles exhibit slight agglomeration, which can be attributed to the magnetic nature and high surface energy of ferrite nanoparticles. The surface appears moderately compact with particles forming small clusters.

The SEM micrograph of 6% Ag-doped $MgFe_2O_4$ (A2) indicates that the spherical morphology is retained after silver incorporation. However, a slight increase in agglomeration is observed compared to the pure sample. The particles appear more closely packed, suggesting that the addition of silver influences particle growth and enhances interparticle interactions. Despite this, the nanoparticles remain within the nanoscale range.

For 9% Ag-doped $MgFe_2O_4$ (A3)**,** the SEM image shows further increase in particle clustering along with minor variation in particle size. The nanoparticles continue to exhibit predominantly spherical shape, but denser agglomeration is noticeable at higher silver concentration. This increased clustering may result from enhanced grain growth and stronger particle interactions during calcination due to higher dopant content.

Overall, the SEM observations confirm that all samples exhibit spherical nanosized particles, while increasing Ag concentration leads to gradual enhancement in agglomeration and particle compactness without significantly altering the basic morphology of $MgFe_2O_4$ nanoparticles.

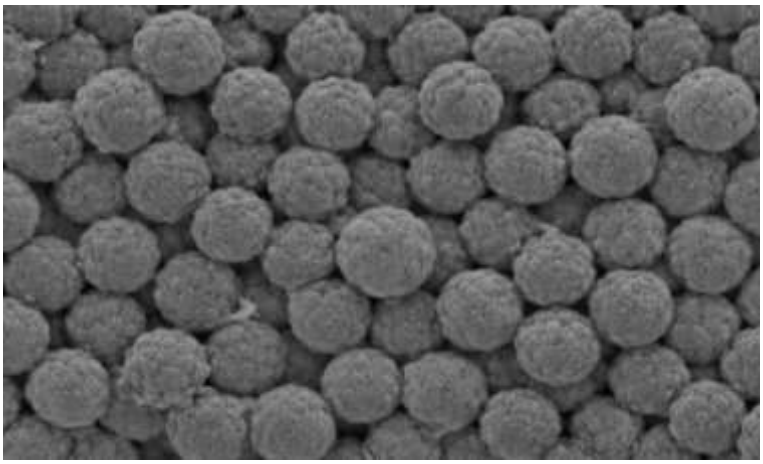

Figure 2 (a) SEM micrograph of pure $MgFe_2O_4$ nanoparticles

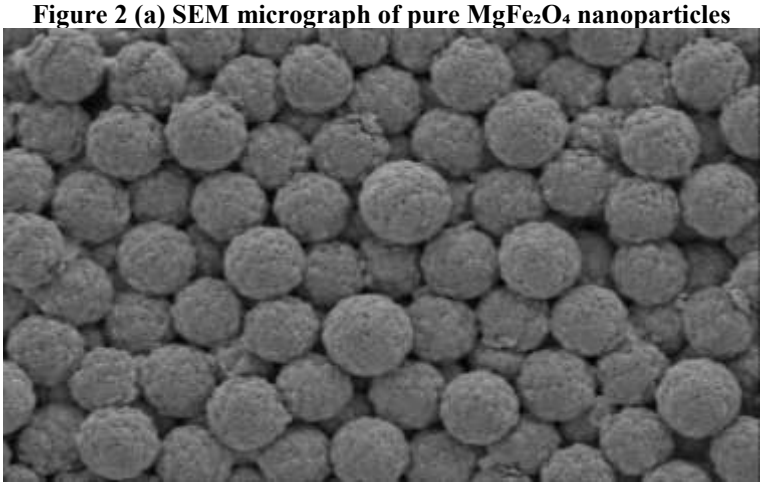

Figure 2 (b) SEM micrograph of 6% Ag-doped $MgFe_2O_4$ nanoparticles

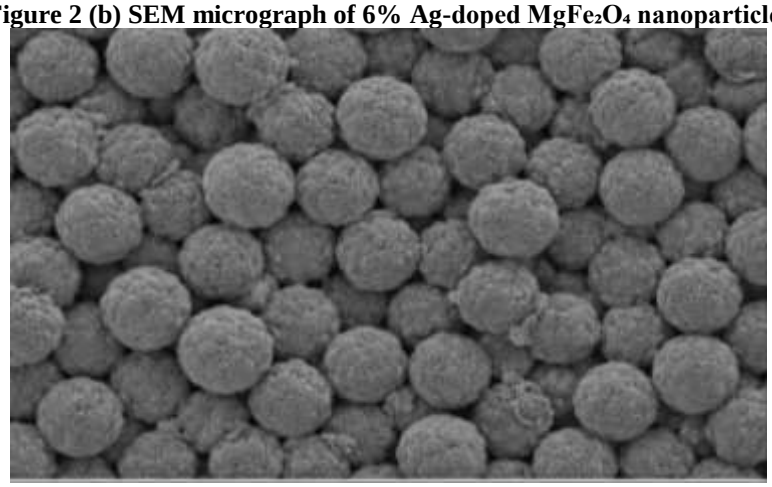

Figure 2 (c) SEM micrograph of 9% Ag-doped $MgFe_2O_4$ nanoparticles

3.3 UV visible spectroscopy

The UV–Visible absorption spectra shown in Figure 3 (a) reveals that all synthesized ferrite samples exhibit strong optical absorption in the visible region, indicating their suitability for photocatalytic and optoelectronic applications. Pure $MgFe_2O_4$ displays comparatively lower absorbance intensity throughout the wavelength range, whereas Ag-doped $MgFe_2O_4$ samples show enhanced absorption behavior. The increase in absorbance with Ag incorporation suggests improved interaction of incident light with the ferrite structure.

The tauc plots presented in Figure 3 (b) were used to determine the optical band gap energy of the synthesized samples using the relation $(\alpha h\nu)^{1/2}$ versus hv. The extrapolation of the linear region of the plots toward the energy axis indicates a gradual reduction in band gap energy after Ag doping. Pure $MgFe_2O_4$ exhibits a relatively larger band gap, while Ag-doped samples show a noticeable

shift toward lower energy values. The reduction in band gap may be associated with the introduction of impurity energy levels, lattice distortion, and enhanced electron transition probability caused by dopant incorporation. All the samples have visible range band gap energy, which facilitates improved visible-light absorption and enhanced charge carrier mobility.

The observed enhancement in optical absorption and narrowing of band gap energy confirms that dopant incorporation plays a significant role in tuning the optical properties of magnesium ferrite nanoparticles. These modifications are highly beneficial for photocatalytic degradation, solar energy conversion, and other light-driven environmental applications due to improved visible-light responsiveness and efficient charge separation characteristics.

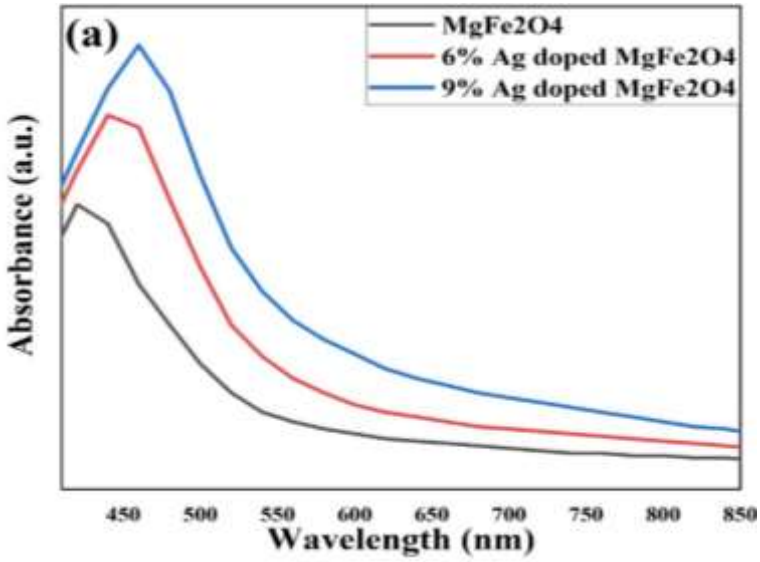

Figure 3 (a) UV- Visible absorbance spectras

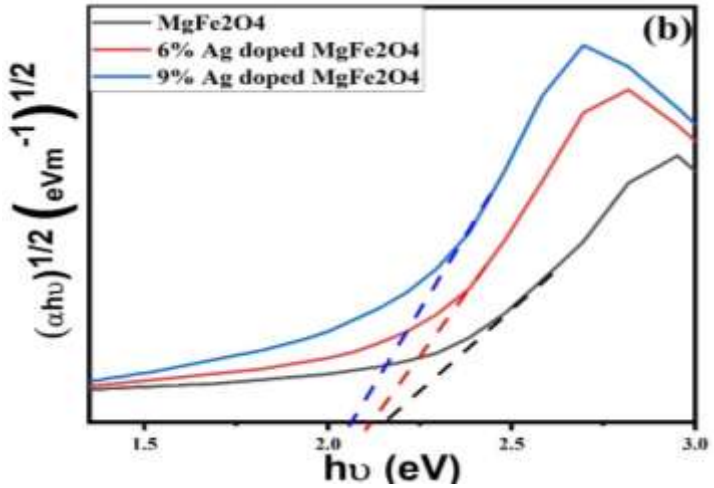

Figure 3 (b) Corresponding Tauc Plots

3.4 BET Analysis

Figure 4 (a-c) displays BET adsorption–desorption measurements were performed to evaluate the surface properties and pore structure of the synthesized ferrite nanoparticles. All samples displayed Type-IV adsorption isotherms with noticeable hysteresis loops, confirming the formation of mesoporous structures. The hysteresis behavior indicates capillary condensation within interconnected pores generated by nanosized particle assembly and intergranular voids.

The calculated BET parameters reveal a significant variation in surface characteristics among the prepared samples. Sample T2 exhibited the maximum specific surface area of 40.3 m^2/g along with the highest pore volume of 1.22 cm^3/g. The increase in these values suggests the development of a highly porous framework with a larger number of accessible active sites. Such enhancement may be associated with the influence of dopant incorporation, which suppresses excessive crystal growth and improves pore formation during thermal treatment.

Sample T3 also demonstrated enhanced mesoporosity with a surface area of 38.4 m^2/g and pore volume of 0.94 cm^3/g. Although slightly lower than T2, the results indicate the presence of well-connected mesoporous channels favorable for adsorption and catalytic reactions. On the other hand, T1 showed the lowest surface area of 30.2 m^2/g and a pore volume of 0.05 cm^3/g, reflecting comparatively dense particle packing and reduced pore development.

The increase in surface area and pore volume observed for the doped samples is expected to improve photocatalytic efficiency by providing more adsorption sites and facilitating rapid diffusion of reactant molecules. The BET results therefore demonstrate that modification of $MgFe_2O_4$ nanoparticles effectively enhances their textural properties, making them suitable for photocatalytic dye degradation and other environmental applications.

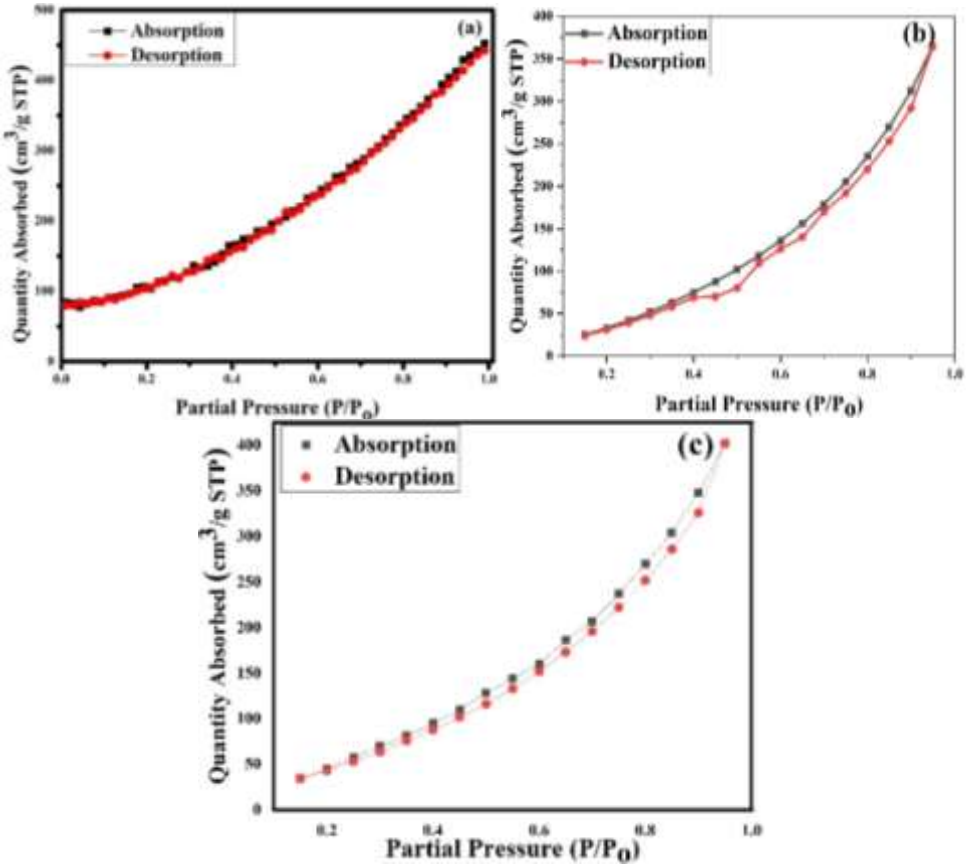

Figure 4 BET isotherm plots of samples

Table 2: BET Surface area, Pore Volume and Band gap energy of nanoparticles

Sample	Surface Area (m^2/g)	Pore Volume (cm^3/g)	Band gap energy (eV)
T1	30.2	0.05	~ 2.1
T2	40.3	1.22	2.11
T3	38.4	0.94	2.06

3.5 Photocatalytic Degradation of Congo Red Dye Analysis

The photocatalytic degradation efficiency of pure $MgFe_2O_4$, 6% Ag-doped $MgFe_2O_4$, and 9% Ag-doped $MgFe_2O_4$ nanoparticles as a function of irradiation time is presented in Figure 5. The degradation percentage increases steadily with irradiation time for all samples, indicating progressive decomposition of the dye under visible light illumination.

Pure $MgFe_2O_4$ exhibits comparatively lower photocatalytic performance, achieving approximately 50% degradation after 150 minutes of irradiation. The slower degradation rate may be attributed to rapid recombination of photogenerated electron–hole pairs and limited visible light absorption.

In contrast, Ag-doped samples demonstrate significantly enhanced photocatalytic activity. The 6% Ag-doped $MgFe_2O_4$ sample shows the highest degradation efficiency, reaching nearly complete degradation (~100%) within 150 minutes. This improvement can be attributed to the presence of silver ions, which act as electron traps, reducing charge carrier recombination and enhancing visible light absorption.

The 9% Ag-doped $MgFe_2O_4$ sample also exhibits improved photocatalytic performance compared to pure $MgFe_2O_4$, achieving around 85–90% degradation after 150 minutes. However, its efficiency is slightly lower than that of the 6% Ag-doped sample. This reduction at higher doping concentration may be due to excessive silver content, which can lead to particle agglomeration and the formation of recombination centers, thereby decreasing photocatalytic efficiency.

Overall, the results indicate that Ag doping significantly enhances photocatalytic activity, with 6% Ag-doped $MgFe_2O_4$ showing optimum performance. The improved degradation efficiency is mainly attributed to enhanced charge separation, increased surface activity, and better visible light utilization.

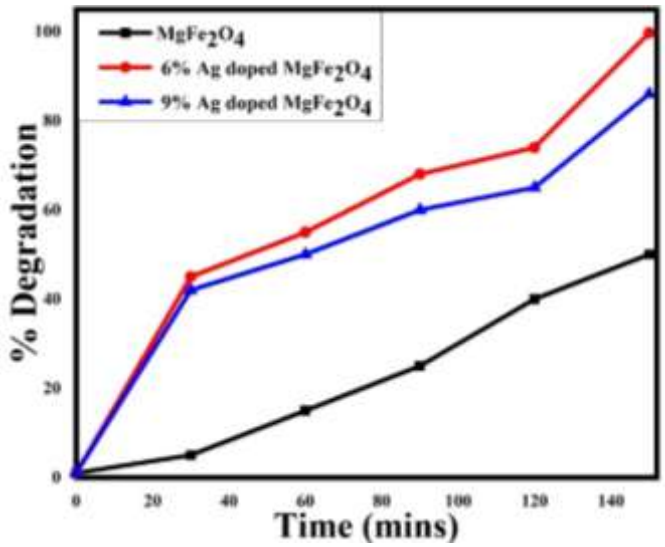

Figure 5. Photocatalytic degradation efficiency of pure $MgFe_2O_4$, 6% Ag-doped $MgFe_2O_4$, and 9% Ag-doped $MgFe_2O_4$ nanoparticles under visible light irradiation

Table 3 Photocatalytic Outcomes in 150 mins

Sample	% Degradation (150 mins) (Congo Red dye)	Performance
A1	48	Low
A2	99.7	Highest
A3	86	Moderate

Conclusions

In the present investigation, pure and Ag-doped $MgFe_2O_4$ nanoparticles were successfully synthesized and their structural, surface, optical, morphological, and photocatalytic properties were systematically examined. XRD analysis confirmed the formation of single-phase cubic spinel ferrite structure for all synthesized samples. The gradual decrease in crystallite size from 31.8 nm to 17.6 nm with increasing Ag concentration indicates that silver incorporation effectively restricts crystal growth. Minor variations in lattice parameter and microstrain further suggest successful dopant substitution within the $MgFe_2O_4$ lattice.

BET analysis revealed that Ag doping significantly enhanced the textural properties of the nanoparticles. The increase in surface area and pore volume confirms the development of mesoporous structure, which provides a larger number of active sites for catalytic reactions. UV–Visible studies demonstrated strong absorption in the visible region along with a slight reduction in band gap energy, indicating improved visible-light harvesting ability after doping. SEM observations showed the formation of spherical nanosized particles, while higher Ag concentration resulted in increased agglomeration and particle compactness.

The photocatalytic performance evaluated using Congo Red dye degradation under visible-light irradiation showed remarkable improvement for doped samples. Among all the synthesized materials, sample 6% Ag doped $MgFe_2O_4$ exhibited the highest degradation efficiency of 99.7% within 150 minutes, which can be attributed to its optimum surface area, reduced crystallite size, enhanced porosity, and improved optical absorption. The overall study confirms that Ag doping plays an important role in tuning the physicochemical properties of $MgFe_2O_4$ nanoparticles and significantly enhances their photocatalytic efficiency. Therefore, Ag-doped $MgFe_2O_4$ nanoparticles can be considered promising materials for wastewater treatment and environmental remediation applications.

Acknowledgment

The authors would like to express their sincere gratitude to IEC University for providing the necessary characterization facilities, infrastructure, and institutional support required for carrying out this research work. The authors also extend their heartfelt thanks to the Department of Physics, National Institute of Technology Kurukshetra, for their valuable technical assistance and support during the characterization and analysis of the samples. The cooperation and encouragement received from both institutions are gratefully acknowledged.

References

1. Solayman, H. M., et al. “Performance Evaluation of Dye Wastewater Treatment Technologies: A Review.” Journal of Environmental Chemical Engineering, vol. 11, no. 3, 2023, p. 109610.

2. Donkadokula, N. Y., et al. “A Review on Advanced Physico-Chemical and Biological Textile Dye Wastewater Treatment Techniques.” Reviews in Environmental Science and Bio/Technology, vol. 19, no. 3, 2020, pp. 543–560.

3. Adesanmi, B. M., et al. “Comparison of Dye Wastewater Treatment Methods: A Review.” GSC Advanced Research and Reviews, vol. 10, no. 2, 2022, p. 126.

4. Chethana, M., et al. “Green Approach to Dye Wastewater Treatment Using Biocoagulants.” ACS Sustainable Chemistry & Engineering, vol. 4, no. 5, 2016, pp. 2495–2507.

5. Kumari, H., et al. “A Review on Photocatalysis Used for Wastewater Treatment: Dye Degradation.” Water, Air, & Soil Pollution, vol. 234, no. 6, 2023, p. 349.

6. Wang, X., Zhu, N., and Yin, B. "Preparation of Sludge-Based Activated Carbon and Its Application in Dye Wastewater Treatment." Journal of Hazardous Materials, vol. 153, no. 1–2, 2008, pp. 22–27.
7. Koe, W. S., et al. "An Overview of Photocatalytic Degradation: Photocatalysts, Mechanisms, and Development of Photocatalytic Membrane." Environmental Science and Pollution Research, vol. 27, no. 3, 2020, pp. 2522–2565.
8. Bhatkhande, D. S., Pangarkar, V. G., and Beenackers, A. A. C. M. "Photocatalytic Degradation for Environmental Applications—A Review." Journal of Chemical Technology & Biotechnology, vol. 77, no. 1, 2002, pp. 102–116.
9. Akpan, U. G., and Hameed, B. H. "Parameters Affecting the Photocatalytic Degradation of Dyes Using TiO_2-Based Photocatalysts: A Review." Journal of Hazardous Materials, vol. 170, no. 2–3, 2009, pp. 520–529.
10. Kumar, A., and Pandey, G. "A Review on the Factors Affecting the Photocatalytic Degradation of Hazardous Materials." Materials Science and Engineering International Journal, vol. 1, no. 3, 2017, pp. 1–10.
11. Rauf, M. A., and Ashraf, S. S. "Fundamental Principles and Application of Heterogeneous Photocatalytic Degradation of Dyes in Solution." Chemical Engineering Journal, vol. 151, no. 1–3, 2009, pp. 10–18.
12. Sakkas, V. A., et al. "Photocatalytic Degradation Using Design of Experiments: A Review and Example of the Congo Red Degradation." Journal of Hazardous Materials, vol. 175, no. 1–3, 2010, pp. 33–44.
13. Reza, K. M., Kurny, A. S. W., and Gulshan, F. "Parameters Affecting the Photocatalytic Degradation of Dyes Using TiO_2: A Review." Applied Water Science, vol. 7, no. 4, 2017, pp. 1569–1578.
14. Viswanathan, B. "Photocatalytic Degradation of Dyes: An Overview." Current Catalysis, vol. 7, no. 2, 2018, pp. 99–121.
15. Ahmed, S., et al. "Advances in Heterogeneous Photocatalytic Degradation of Phenols and Dyes in Wastewater: A Review." Water, Air, & Soil Pollution, vol. 215, no. 1, 2011, pp. 3–29.
16. Bielan, Z., et al. "Application of Spinel and Hexagonal Ferrites in Heterogeneous Photocatalysis." Applied Sciences, vol. 11, no. 21, 2021, p. 10160.
17. Ma, H., and Liu, C. "A Mini-Review of Ferrites-Based Photocatalyst on Application of Hydrogen Production." Frontiers in Energy, vol. 15, no. 3, 2021, pp. 621–630.
18. Rahman, A., and Jayaganthan, R. "Photocatalytic Studies of Composite Ferrite Nanoparticles." Russian Journal of Inorganic Chemistry, vol. 64, no. 7, 2019, pp. 946–954.
19. Singh, G., et al. "A Review on Impacting Parameters for Photocatalytic Degradation of Organic Effluents by Ferrites and Their Nanocomposites." Processes, vol. 11, no. 6, 2023, p. 1727.
20. Skliri, E., et al. "Assembly and Photochemical Properties of Mesoporous Networks of Spinel Ferrite Nanoparticles for Environmental Photocatalytic Remediation." Applied Catalysis B: Environmental, vol. 227, 2018, pp. 330–339.
21. Lagashetty, A., Pattar, A., and Ganiger, S. K. "Synthesis, Characterization and Antibacterial Study of Ag Doped Magnesium Ferrite Nanocomposite." Heliyon, vol. 5, no. 5, 2019.
22. Shetty, K., et al. "Photocatalytic Study for Fabricated Ag Doped and Undoped $MgFe_2O_4$ Nanoparticles." Materials Today: Proceedings, vol. 4, no. 11, 2017, pp. 11764–11772.